Behavior of Doped Hydroxyapatites During the Heat Treatment

FIRUTA GOGA[1], EDIT FORIZS [1], GEORGE BORODI[2], GHEORGHE TOMOAIA[3,4], ALEXANDRA AVRAM[1], REKA BALINT[1], AURORA MOCANU[1], OSSI HOROVITZ[1], MARIA TOMOAIA COTISEL[1,4,*]

[1]Babes Bolyai University of Cluj Napoca, Faculty of Chemistry and Chemical Engineering, Physical Chemistry Centre, Chemical Engineering Department, 11 Arany J. Str., 400084, Cluj Napoca, Romania

[2]National Institute for Research and Development of Isotopic and Molecular Technologies, 65-103 Donath Str., 400293, Cluj Napoca, Romania

[3]Iuliu Hatieganu University of Medicine and Pharmacy, Orthopedics and Traumatology Department, 47 Traian Mosoiu Str., 400132, Cluj Napoca, Romania

[4]Academy of Romanian Scientists, 54 Splaiul Independentei, 050094, Bucharest, Romania

The goal of this investigation is related to the development of nanostructured biomaterials based on hydroxyapatite (HAP) and multi-doped hydroxyapatites (HAPs), with essential physiological elements, like Mg, Zn, Sr, and Si, for bone repair and regeneration. Nano hydroxyapatites pastes and powders were obtained by wet chemical method using innovative nanotechnology and advanced processing of biomaterials at various temperatures to control the crystallite size and crystallinity degree. The prepared HAPs were analysed by various physical and chemical methods, like SEM, SEM-EDX, AFM, XRD, TG and DSC analysis. The results showed that these biomaterials both in pastes and in powders contained a unique phase, characterized by the HAP structure, which was substantially preserved even at 1000 °C, indicating a high thermal stability of these biomaterials. To enhance their usage, we have prepared HAP and multi-doped HAPs in the form of pastes with controlled humidity (moisture) and powders with controlled crystallinity, which were lyophilized or lyophilized calcined at 300 °C for 1 h. Preliminary biological tests showed that the adhesion and proliferation of human osteoblasts depended on the heat treatment of HAPs used for building the scaffolds. The findings suggest that these biomaterials based on HAPs may have a wide range of medical applications as bone substitute and coatings on metallic implants.

Keywords: nano hydroxyapatite, doped hydroxyapatites, essential physiological elements, XRD, SEM-EDX, AFM, thermal analysis

It is recognized that biomaterials based on hydroxyapatite [HAP, $Ca_{10}(PO_4)_6(OH)_2$] possess high biocompatibility and good bioactivity, and can stimulate osteoconduction, being slowly replaced by the host bone after implantation [1-3]. They are potential alternatives as bone grafts for medical applications and as coatings for metallic implants [1].

Doped hydroxyapatites [[HAPs] with Sr [2- 6], Mg [2, 7, 8], Si [9-11] and Zn [2, 11, 12] have the advantage that they inherit the HAP structure and some biological properties of doping elements, that intervene in bone development and metabolism.

The major advantage of strontium is that it reduces bone resorption and enhances bone formation [4], and thus, it is a promising element for the treatment of osteoporosis [5]. Magnesium has an important role in biological systems and plays a structural role in bone development [7]. Silicon is important in calcifying process of bones [9], and stimulates osteoblasts in bone formation [10]. Zinc is an element with diverse role in biological functions and stimulates the regeneration of bone tissues, increases bone density and reduces bone loss [11-13]. Titanium implants coated with Zn, Mg and Sr doped hydroxyapatite showed an improvement in their osseointegration process, particularly for those coatings with 10% Sr content [14]. Different records also showed an enhancement in corrosion resistance [15] or in antibacterial activity [16] for coatings containing Sr on metallic implants.

Due to various benefits, the research is continuously focused on simultaneous incorporation of two or more substituents in hydroxyapatite lattice [11, 17-24] for obtaining the best characteristics for biomedical applications.

At least three types of HAPs can be pointed out, namely as pastes, as granulated lyophilized powders, and as porous calcined, lyophilized powders useful in bone repair and regeneration, and as coatings for surgical applications. Certainly, these applications involve a treatment of the obtained biomaterials at elevated temperatures, which is the basis of our motivation in the present study.

The important objective was to explore the thermal stability of HAPs multi doped with essential physiological elements, like magnesium, zinc, strontium and silicon, at high temperature up to 1000 °C. The goal of this work was also to investigate the effect of simultaneous doping with the four elements, Mg, Zn, Sr and Si (HAP-Mg-Zn-Sr-Si), within HAP lattice on the structure and thermal behavior of synthesized HAPs biomaterials. The obtained biomaterials were investigated by thermogravimetric (TG / DTG) analysis, differential scanning calorimetry (DSC), X-ray diffraction (XRD), scanning electron microscopy (SEM), energy-dispersive X-ray (EDX) elemental analysis and atomic force microscopy (AFM).

Experimental part

Materials and methods

The following compounds $Ca(NO_3)_2 \cdot 4H_2O$, $(NH_4)_2HPO_4$, $Mg(NO_3)_2 \cdot 6H_2O$, $Zn(NO_3)_2 \cdot 6H_2O$, $Sr(NO_3)_2$ and tetraethyl orthosilicate $(C_2H_5O)_4Si$, TEOS) were used as starting materials, as Ca, P, Mg, Zn, Sr and Si precursors. Pure stoichiometric HAP and three doped hydroxyapatites with constant content of Mg, Zn and Si (table 1) and two different contents in Sr were prepared using a wet precipitation method, developed previously by us [6, 10, 12]. All chemicals were reagent grade and purchased form

* email: mcotisel.chem.ubbcluj.ro@gmail.com

Merck and Sigma-Aldrich. All solutions were prepared with double distilled water, which was further deionized in Elgastat purification system.

Synthesis of pure HAP and doped HAP

A pure HAP paste was obtained by wet precipitation method. A *solution 1*, comprising 0.25 M Ca^{2+} was prepared by dissolving the calculated amount of $Ca(NO_3)_2 \cdot 4H_2O$ in ultrapure water. The 25% ammonia solution was added to assure a pH value of 11.5. A *solution 2* was made, comprising 0.15 M PO_4^{3-}, which was obtained by dissolving $(NH_4)_2HPO_4$ in ultrapure water, and the *p*H was fixed at 11.5 by adding 25% ammonia solution. Equal volumes of these two solutions were mixed at 22°C, assuring a mole ratio Ca /P of 5/3 (1.67), characteristic for stoichiometric HAP. A reasonably intensive mixing was assured using a peristaltic pump Masterflex L/S Digital Drive, 600 RPM, 115/230 VAC, EW-07523-80, and an impact reactor type Y for the two liquid flows. The reaction mixture was aged in two steps, for 24 h at 22°C, followed by 24h at about 70 °C, under stirring. The precipitated solid phase was vacuum filtered, washed in distilled water until free of nitrate ions and the supernatant was neutral (*p*H 7). This wet precipitate, named also paste, was used as it is or was freeze-dried in lyophilizer equipment Martin Christ, model Alpha 1-4 LDplus. Finally it was ground using an agate mortar and was used as lyophilized powder. Further, this lyophilized powder was calcined at 300 °C for 1h.

The multi-substituted hydroxyapatites were obtained in an analogue manner, the only difference being the composition of the two initial solutions. *Solution 1* contained the cations (0.25 M in $Ca^{2+}+Mg^{2+}+Zn^{2+}+Sr^{2+}$) and was obtained from the corresponding nitrates $Ca(NO_3)_2 \cdot 4H_2O$, $Mg(NO_3)_2 \cdot 6H_2O$, $Zn(NO_3)_2 \cdot 6H_2O$ and $Sr(NO_3)_2$ (all from Sigma-Aldrich, Steinheim, Germany), dissolved in ultrapure water, in the ratios required by the composition of the final doped HAP biomaterial. The anions containing *solution 2* (0.15 M in $PO_4^{3-}+SiO_4^{4-}$) was obtained from $(NH_4)_2HPO_4$, and tetraethyl orthosilicate, TEOS, (as source for silicate ions), both dissolved in ultrapure water, in the ratios required by the composition of the selected product. The *p*H was settled at 11.5 by adding a 25% ammonia solution. Solutions 1 and 2 (equal volumes) were mixed at 22°C, so the mole ratio (Ca+Mg+Zn+Sr)/(P+Si) was maintained at the value 5/3 (1.67). The subsequent maturation was achieved in two stages, under intermittent stirring: 24 h at 22°C, and 24h at 70°C. The processing of the obtained pastes (wet precipitates) was the same as in the case of pure HAP.

Finally, 12 biomaterials were obtained, namely four pastes, four lyophilized powders, and four powders calcined at 300°C for 1h. These biomaterials were morphologically and structurally characterized and their thermal stability was determined.

Characterisation methods

Thermal behaviour of pure HAP and doped HAP powders was determined by thermogravimetric analysis (TGA) and DSC analysis, for the temperature range from 25 to 1000 °C, using Universal SDTQ600 TA Instruments. Samples were heated in alumina crucibles at a constant heating rate of 10°C/min, in flowing air, using simultaneous TG/DTG-DTA/DSC techniques.

X-Ray diffractions (XRD) were carried out using a Bruker D8 Advance diffractometer, in Bragg-Brentano geometry, equipped with a X-ray tube with copper K_a line, wavelength 1.541874 Å). Phases were identified by comparing the peak positions of the diffraction patterns with standard PDF patterns.

Field emission *scanning electron microscope* (*SEM*), Hitachi SU-8230, operated at 30 kV, is used to explore the morphology of synthesized HAPs biomaterials. SEM is equipped with Oxford energy-dispersive X-ray spectrometer (EDS) for elemental analysis (SEM-EDX). SEM grids are made of Cu, covered by a carbon layer of 10 to 20 nm thickness. SEM samples were prepared by deposition of HAP samples, either as wet precipitate (paste) or powder, in thin layers on SEM grids. For high contrast the samples were covered by a thin layer of gold.

Atomic force microscopy (AFM) images were obtained using the AFM JEOL 4210 equipment, operated in tapping mode [25-28], using standard cantilevers with silicon nitride tips (resonant frequency in the range of 200-300 kHz, and spring constant 17.5 N/m). The particles were adsorbed from their aqueous dispersion for 20 s on optically polished glass support.

Results and discussions

Composition of synthesized pastes and powders

For Ca substitution simultaneously with Mg, Zn and Sr, the $(Ca^{2+} + Mg^{2+} + Zn^{2+} + Sr^{2+})/PO_4^{3-}$ ratio was maintained at 1.67 for all samples, which is the stoichiometric value for HAP structure. The element content is given in weight % and in the moles of element/ mole HAP, shown in Table 1, for all synthesized HAPs. The HAPc is the triple substituted HAP with Mg, Zn and Si, (HAP-Mg-Zn-Si). The four doped HAP, (HAP-Mg-Zn-Sr-Si), is noted HAPc-Sr, and it is synthesized for 2 different Sr contents, namely 5 wt% and 10wt% Sr, respectively.

SEM images of HAPs, pastes and powders

SEM images are used to observe the morphology, texture and particles of HAPs biomaterials and energy-dispersive X-ray (EDX) spectra are used for chemical analysis of all HAP samples.

Figure 1 (a-d) shows SEM images for the four HAPs pastes. The morphology was slightly similar, rather compact presenting irregular, agglomerated structures made of spherical particles. The histograms of size distribution of particles are also shown for each paste. The average diameters of constitutive particles indicate an almost identical value of about 14 nm for all pastes. However, a slight tendency of different arrangements of particles in various pastes appears like in HAPc when compared with pure HAP or with HAPc-Sr. This situation

Table 1

COMPOSITION OF SYNTHESIZED HYDROXYAPATITE SAMPLES (HAPs) AND THEIR THEORETICAL FORMULA

No.	Sample	Mg wt%	Zn wt%	Sr wt%	Si wt%	Theoretical formula
1	HAP	0	0	0	0	$Ca_{10}(PO_4)_6(OH)_2$
2	HAPc	1.5	0.2	0	0.2	$Ca_{9.36}Mg_{0.61}Zn_{0.03}(PO_4)_{5.93}(SiO_4)_{0.07}(OH)_{1.93}$
3	HAPc-5% Sr	1.5	0.2	5	0.2	$Ca_{8.76}Mg_{0.63}Zn_{0.03}Sr_{0.58}(PO_4)_{5.93}(SiO_4)_{0.07}(OH)_{1.93}$
4	HAPc-10% Sr	1.5	0.2	10	0.2	$Ca_{8.12}Mg_{0.65}Zn_{0.03}Sr_{1.20}(PO_4)_{5.93}(SiO_4)_{0.07}(OH)_{1.93}$

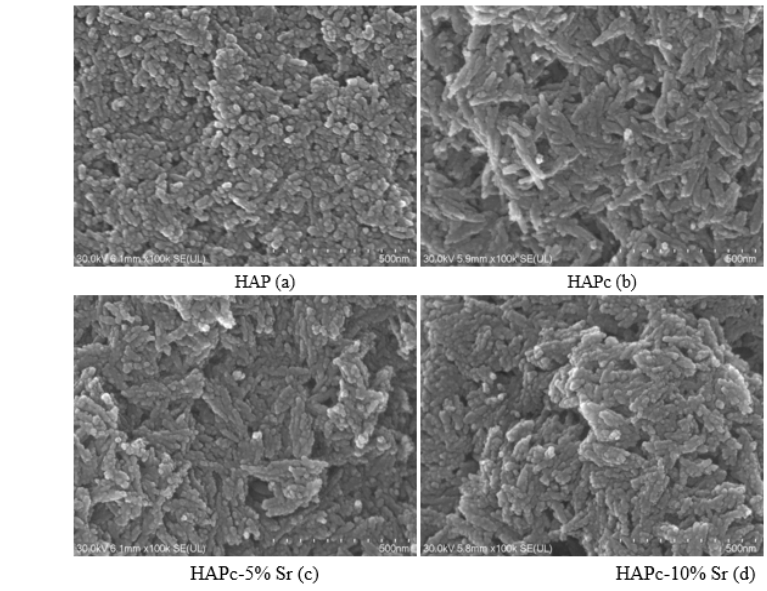

Fig. 1. SEM images for pastes of HAP (a), HAPc (b), HAPc-5% Sr (c), and HAPc-10% Sr (d) and corresponding histograms of size distribution of particles

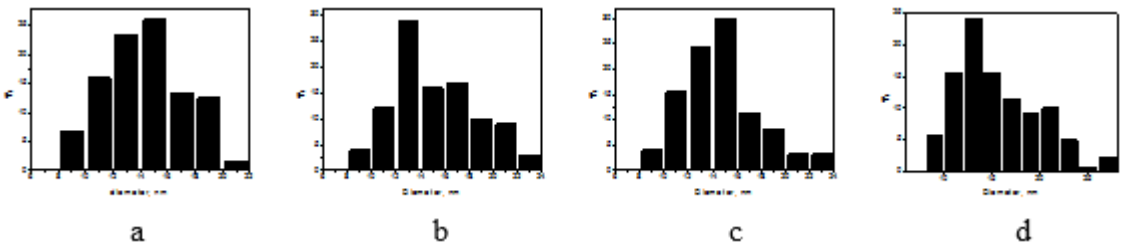

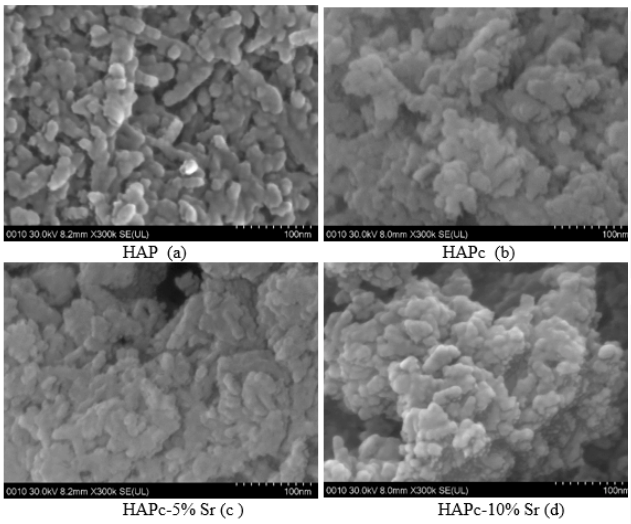

Fig. 2. SEM images for calcined lyophilized powders of HAP (a), HAPc (b), HAPc-5% Sr (c), and HAPc-10% Sr (d), at 300 °C for 1h; bars in images are 100 nm

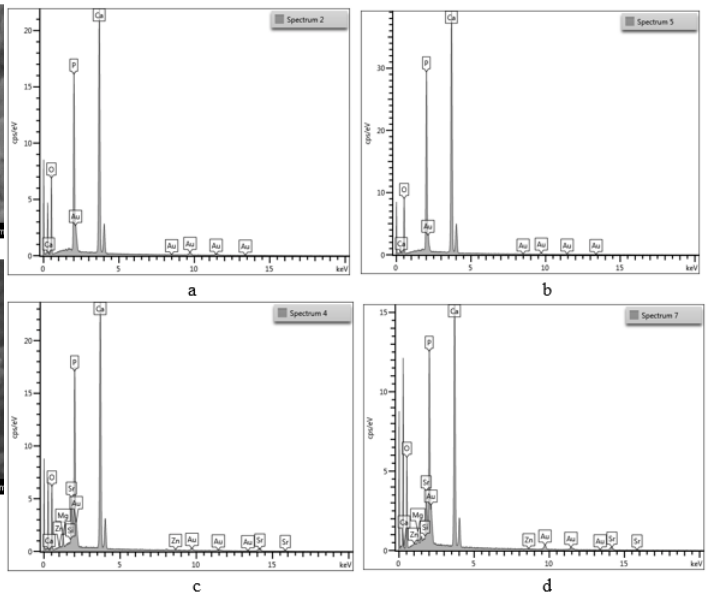

Fig. 3. EDX spectra for HAP powders: lyophilized (a) and calcined lyophilized (b); for HAPc-10%Sr: lyophilized (c) and calcined lyophilized (d); calcined samples at 300 °C for 1h

can explain a different water quantity preserved in various pastes, depending on the chemical composition of biomaterial and on the ions existing at the interface among particles and surrounding water molecules. The HAPs particles are relatively distinct and form clusters of self-assemblies.

SEM images were also obtained for lyophilized powders and on calcined lyophilized powders for the eight biomaterials. For example, figure 2 gives the morphology for calcined lyophilized HAPs powders, calcined at 300 °C for 1 h. Analyzing SEM images, a porous structure is observed, and the packing of particles seems significantly different than those for the morphology of pure HAP, depending on the composition of the biomaterial.

The elemental composition in the synthesized HAPs biomaterials was assessed by using SEM-EDX spectra, recorded on 10 different areas of each sample. For example, figure 3 presents EDX spectra for pure HAP powders (figs. 3a and 3b), and for doped HAPc-10%Sr powders (figs. 3c and 3d), of two types, lyophilized and calcined lyophilized. The identification of peaks for constitutive elements confirms the formation of doped HAPs. Additional peaks for gold are related with the gold layer that covered the sample for SEM imaging. The formation of doped HAPs is well supported by the presence of all elements including the peak for oxygen.

Moreover there is a very good accord between measured (EDX spectra) and calculated (table 1) content for each constituent element, indicating a unique structure and a homogeneous composition within these biomaterials. The mole ratio of the total amount of cations (Ca^{2+} + Mg^{2+} + Zn^{2+} + Sr^{2+}) to the amount of anions (PO_4^{3-}+ SiO_4^{4-}) for all samples is almost near to the theoretical value (1.67) characteristic for the hydroxyapatite structure.

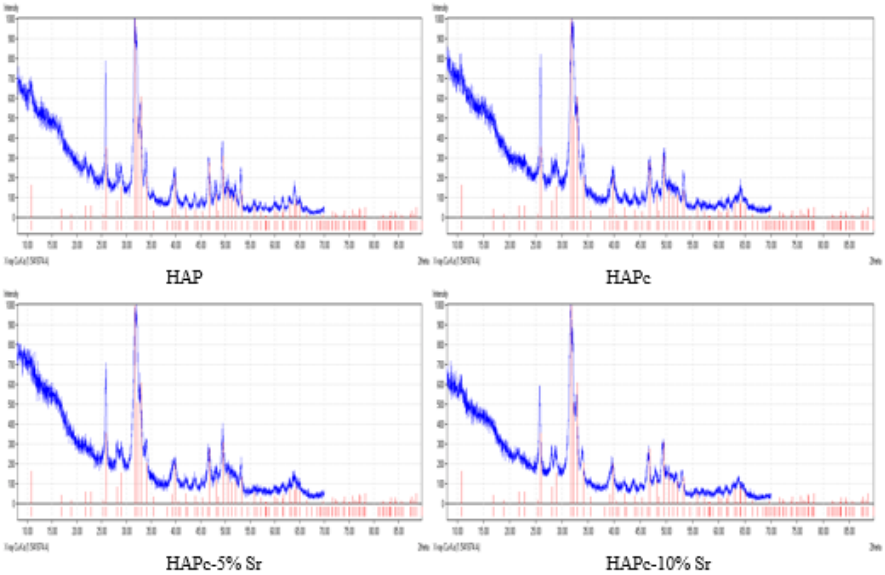

Fig. 4. Experimental XRD patterns (blue lines) for calcined lyophilized powders: HAP, HAPc, HAPc-5% Sr, and HAPc-10% Sr, at 300 °C for 1h, compared with standard PDF patterns 74-0566 of stoichiometric HAP (red lines).

XDR for calcined lyophilized powders

The XRD patterns of the HAPs powders are given in figure 4, as an example for HAP, HAPc, HAPc-5%Sr, HAPc-10%Sr, lyophilized powders, calcined at 300 °C for 1 h. All peaks positions are in substantial agreement with those correspmding to the standard data for pure stoichiometric HAP (standard PDF patterns No. 74-0566), and no other peaks are found to be attributed to a secondary phase along with HAP structure.

Further, for HAPc-10%Sr the peak positions are slightly shifted (in the 2ϑ values) towards the lower angles from the standard patterns for pure stoichimetric HAP, suggesting the substitution of Sr into HAP lattice, as already reported in similar situations [29]. Moreover, the XRD patterns for HAPc-10%Sr are in a very good agreement with the standard data for $Ca_9Sr(PO4)_6(OH)_2$ (standard PDF patterns No. 34-0484), indicating a very good stability of the HAP lattice having Mg, Zn, and Si, beside Sr. This finding justifies the important role of Sr to stabilize the doped HAP structure for:HAP-(1.5%)Mg-(0.2%)Zn-(0.2%)Si–(10%)Sr biomaterial. In this doped HAP structure, there are three cations substituting for Ca^{2+}, in the HAP lattice, and the lower angle shifts are essentially due to the greater ionic radius of Sr^{2+} (than the radius of other cations) substituted in the HAP structure.

The size of crystallites and crystallinity degree for lyophilized powders, further calcined at 300 °C for 1h, for pure hydroxyapatite and multi doped HAPs were determined from XRD patterns (fig. 4) and are given in table 2.

All crystallite sizes are in the nanoscale range, with an average crystallinity degree, which is the highest for pure HAP and the lowest for multi doped HAP. The effect of calcination at 300°C for 1 h was only a slight increase of crystallite size for all obtained nano powders: HAP, HAPc, and for HAPc containing Sr. The crystallinity degree was only slightly increased by calcination in agreement with other similar situations [30].

AFM images of HAPs powders

As an example, AFM images for non calcined lyophilized HAPc-5%Sr powders dispersed in pure water and adsorbed as a self-assembled layer on glass are shown in figure 5. As observed in 2D topography (fig. 5a), phase image (fig. 5b), amplitude image (fig. 5c), 3D-topography (fig. 5d) and in cross profile (fig. 5e), the shape of particles is almost spherical with an average diameter of 39 ± 2 nm.

AFM images also confirmed for all calcined lyophilized powders the average size of particles in the nanoscale range, as following 45 ± 3 nm for HAP, 40 ±2 nm for HAPc, 37 ± 3 nm for HAPc-5%Sr and 35 ±2 nm for HAPc-10%Sr. Notably, AFM images indicated that the nano suspensions of HAPs powders, lyophilized non calcined or lyophilized calcined, are formed of particles of almost identical size in very good agreement with crystallite size determined in XRD data (table 2).

TG and DSC analysis

Figure 6 shows the average weight loss recorded for pastes of HAPs, between 25 and 1000°C, which was 58.82% (HAPc-10% Sr), 61.11 % (HAP), 68.61 % (HAPc-5% Sr) and 70.53% (HAPc). The highest weight loss appeared around 100 °C and can be attributed to very high water content contained within pastes, surrounding HAPs particles. As expected, corresponding DSC data revealed an endothermic DSC transformation for all samples at approximately 100°C (fig. 6). For the temperature interval,

Table 2

THE SIZE OF CRYSTALLITES AND CRYSTALLINITY DEGREE FOR LYOPHILIZED POWDERS, CALCINED AT 300 °C FOR 1H, FOR PURE HAP (SAMPLE 1) AND TRIPLE DOPED HAP: HAPC (SAMPLE 2), AND FOUR DOPED HAP: HAPC-SR (SAMPLES 3 AND 4), DETERMINED FROM XRD PATTERNS (FIG. 4)

Sample	1 HAP	2 HAPc	3 HAPc-5% Sr	4 HAPc-10% Sr
Crystallites size (nm)	46.8	40.7	37.4	34.5
Crystallinity degree (%)	51.2	39.3	39.5	39.0

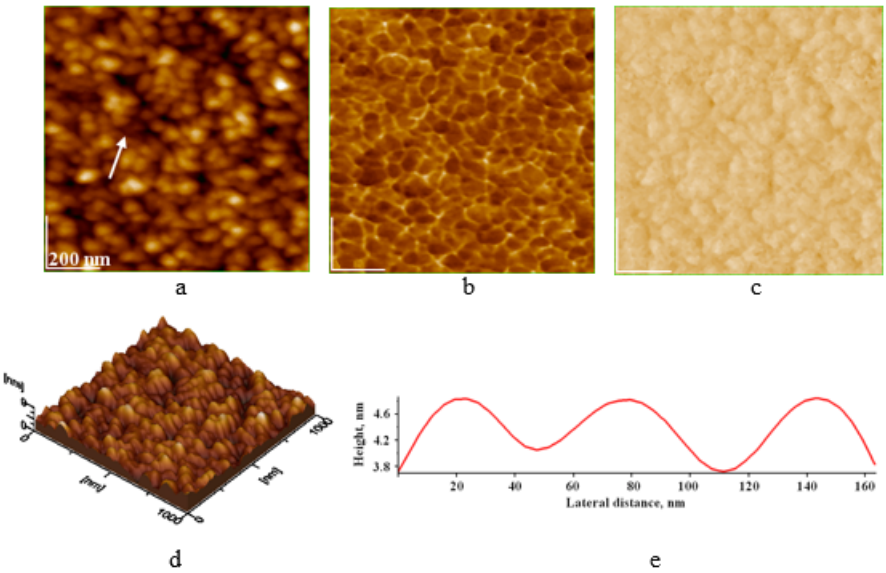

Fig. 5. AFM images for HAPc-5% Sr, lyophilized powders: (a) 2D-topography, (b) phase, (c) amplitude and (d) 3D-topography images; (e) cross section profile along the arrow in panel (a).

from 25 up to 200 °C, the weight loss was 56.31% (HAPc-10% Sr), 60.05% (HAP), 67.21 % (HAPc-5% Sr) and 68.59% (HAPc). After this transformation, from 200 up to 800 °C, the average weight loss was very similar of about 1% for HAP and HAPc-5% Sr, and about 2% for HAPc and HAPc-10% Sr biomaterials. This finding can be associated with the gradual loss of chemically adsorbed water on the surface of HAPs particles, which needs more energy for the release of water from these biomaterials, during the heating. Then, the weight loss, in the interval from 800 up to 1000 °C, is very low of about 0.1% (HAP), 0.2% (HAPc-5% Sr), 0.3% (HAPc), and about 0.4% (HAPc-10% Sr). The initial content of water in these pastes can be controlled by advanced processing and the pastes are very stable, as found for at least one year. The moisture content of these HAPs pastes is comparable with that found in commercial available pure HAP paste.

The average weight loss for powders of HAPs is given in figure7 and figure 8, for non calcined lyophilized powders (fig. 7) and for lyophilized powders, calcined at 300 °C for 1h (fig. 8), for the same interval of temperature between 25 and 1000 °C.

Combined results of TG and DSC (fig. 7) revealed that all HAPs powders have similar TG and DSC curves in this range of temperature. There are three series of mass loss for these biomaterials, namely the range of 25-200, 200-

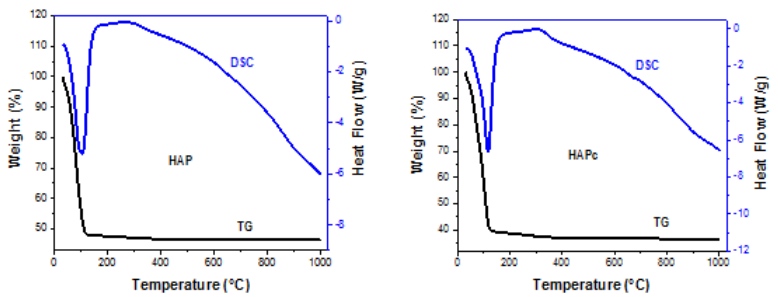

Fig. 6. Thermal behaviour: TG and DSC curves for the four pastes; symbols as in table 1

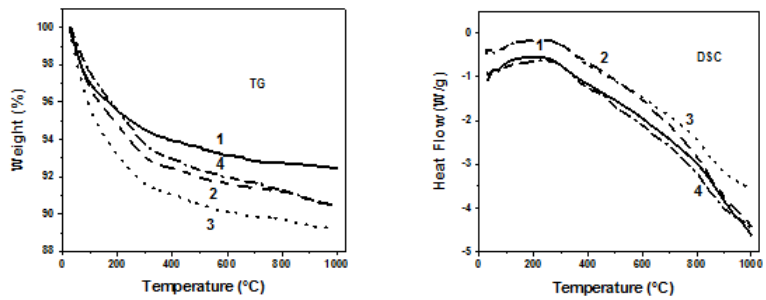

Fig. 7. TG and DSC curves for lyophilized powders: HAP (1); HAPc (2); HAPc-5%Sr (3) and HAPc-10%Sr (4)

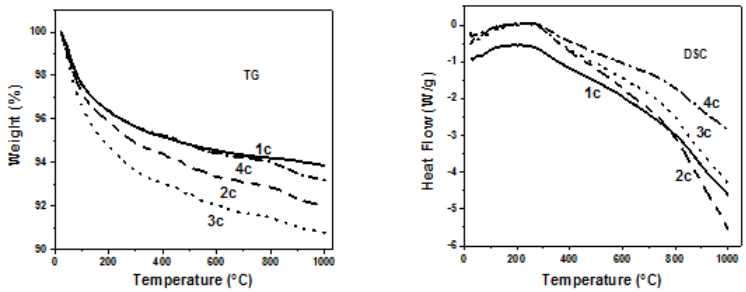

Fig. 8. TG and DSC curves for lyophilized (HAPs) powders, calcined at 300 C for 1h: HAP (1c); HAPc (2c); HAPc-5%Sr (3c) and HAPc-10%Sr (4c)

800 and 800-1000 °C, similarly with found results on pastes of HAPs (fig. 6). The mass loss of about 4.5% for HAP and HAPc-10% Sr, 5.5% for HAPc and 6.8% for HAPc-5% Sr, at 200 °C; about 7% for HAP, 9 % for HAPc-10% Sr and HAPc, and 10 % for HAPc-5% Sr, at 800°C; about 7.7% for HAP, 9.6% for HAPc-10% Sr, 9.8% for HAPc and 10.7 % for HAPc-5% Sr, at 1000 °C. At temperature above 200 °C, the weight loss was higher with roughly 3% for doped HAPs than for pure HAP. Moreover, the TG curves of HAPc and HAP-10%Sr are very similar, while the weight loss for HAPc-5% Sr was about 0.8 % higher than those values corresponding for HAPc and HAPc-10%Sr. These differences among doped HAPs are diminished above 800 °C.

The TG and DSC curves (fig. 8) for HAPs lyophilized and calcined powders are similar with those for lyophilized powders (fig. 7). The TG trend for HAP and HAPc-10% Sr (calcined samples, 1c and 4c) is almost identical up to 800 °C, when the weight loss for doped HAP is somewhat bigger up to about 0.5% (at 1000 °C). Furthermore, the TG curves (fig. 8) are arranged in the same order as that found for lyophilized powders (fig. 7). The unique difference is that the total weight loss for calcined powders was slightly smaller, about 9.3% for HAPc-5% Sr (fig. 8, at 1000°C) compared with 10.7 % recorded for the same biomaterial, but for lyophilized powders (fig. 7, 1000 °C), which might be attributed to a relatively high content of water within these biomaterials.

The nano size of particles, visualized in SEM images (fig. 2) for lyophilized powders, calcined at 300°C, and in AFM images (fig. 5) for lyophilized powders, indicates a potentially large surface area, which may explain the rather high adsorption of water on powder surface within these biomaterials.

In comparison with DSC data for pastes (fig. 6), the predicted endothermic DSC peaks at about 100 °C became very broad for powders (figs. 7 and 8), difficult to be observed in this graphical representation, indicating a relatively low content of humidity for these biomaterials as powders.

The mass loss up to 200 °C may be due to the evaporation of physically adsorbed water on the surface of particles of HAPs in good agreement with thermal analysis of related compounds [2, 3, 31, 32]. The second mass loss from 200 to 800 °C may correspond to desorption of chemically bounded water to the HAPs lattice, which needs more energy to release that water from HAPs structure, as supported by DSC data (figs. 7 and 8). Certainly, water in pores requires more heating to be released due to the capillary effect. Thermal analysis at high temperature might be associated with the gradual loss of lattice water [2, 3, 21, 31- 34]. Above 800 °C up to 1000 °C, the weight loss is insignificant and cannot be attributed to structural decomposition of HAPs biomaterials. Remarkably, a high stability of these synthesized HAPs biomaterials is demonstrated in substantial agreement with reported data for HAP structure [21, 31, 34-39].

Conclusions

Biologically relevant nanomaterials, pure HAP and doped HAP, e.g. HAPc, HAPc-5%Sr, and HAPc-10%Sr, were prepared by wet precipitation method, under identical experimental conditions. The results of structural (XRD), chemical and morphological (SEM, SEM-EDX and AFM) characterization of these nanostructured biomaterials revealed an unique stoichiometric HAP structure of high thermal stability up to 1000 °C. The TG and DSC analysis indicated three stages of thermal behavior of these HAPs, essentially related to the removal of physically adsorbed and chemically bounded water within these materials, without their decomposition up to 1000 °C.

The influence of doping, with Mg, Zn, Sr and Si in the HAP lattice, on biomaterial properties was assessed for crystallite size, crystallinity, and particle morphology, that ultimately can define the biological performance. From our preliminary biological tests, like MTT assay, which measures the activity of mitochondrial dehydrogenase in viable cells, and alkaline phosphatase (ALP) activity, it is clear that human osteoblasts growth, adhesion and proliferation depend on the chemical composition and on the heat treatment of these biomaterials based on doped HAPs, used for building the scaffolds. These findings indicate that these biomaterials are appropriate for bone repair and regeneration and may have medical applications as bone substitute and as coatings on metallic implants.

Acknowledgements: The authors gratefully acknowledge the financial support from the Executive Agency for Higher Education, Research, Development and Innovation Funding (UEFISCDI) through grant no. 241.

References

1. BAYANI, M., TORABI, S., SHAHNAZ, A., POURALI, M., Biotechnol. Biotechnol. Equip., **31**, nr. 2, 2017, p. 215.
2. COX, S.C., JAMSHIDI, P., GROVER, L.M., MALLICK, K.K., Mater. Sci. Eng. C, **35**, 2014, p. 106.
3. OZBEK, Y.Y., BASTAN, F.E., USTEL, F., J. Therm. Anal. Calorim., **125**, 2016, p. 745.
4. MARQUES, C.F., LEMOS, A., VIEIRA, S.I., DA CRUZ E SILVA, O.A.B., BETTENCOURT, A., FERREIRA, J.M.F., Ceram. Int., **42**, 2016, p. 2706.
5. LANDI, E., TAMPIERI, A., CELOTTI, G., SPRIO, S., SANDRI, M., LOGROSCINO, G., Acta Biomater., **3**, 2007, p. 961.
6. FRANGOPOL, P.T., MOCANU, A., ALMASAN, V., GARBO, C., BALINT, R., BORODI, G., BRATU, I., HOROVITZ, O., TOMOAIA-COTISEL, M., Rev. Roum. Chim., **61**, nr. 4-5, 2016, p. 337.
7. LAURENCIN, D., ALMORA-BARRIOS, N., DE LEEUW, N.H., GERVAIS, C., BONHOMME, C., MAURI, F., CHRZANOWSKI, W., KNOWLES, J.C., NEWPORT, R.J., WONG, A., GAN, Z., SMITH, M.E., Biomaterials, **32**, 2011, p.1826.
8. FARZADI, A., BAKHSHI, F., SOLATI-HASHJIN, M., ASADI-EYDIVAND, M., ABU OSMAN, N.A., Ceram. Int., **40**, 2014, p. 6021.
9. QIU, Z.Y., NOH, I.S., ZHANG, S.M., Front. Mater. Sci., **7**, nr. 1, 2013, p.40.
10. TOMOAIA, G., MOCANU, A., VIDA-SIMITI, I., JUMATE, N., BOBOS, L.D., SORITAU, O., TOMOAIA-COTISEL, M., Mater. Sci. Eng. C, **37**, 2014, p.37.

11. SHEPHERD, J.H., SHEPHERD, D.V., BEST, S.M., J. Mater. Sci.: Mater. Med., **23**, nr.10, 2012, p. 2335.
12. GARBO, C., SINDILARU, M., CARLEA, A., TOMOAIA, G., ALMASAN, V., PETEAN, I., MOCANU, A., HOROVITZ, O., TOMOAIA-COTISEL, M., Particulate Sci. Technol., **35**, nr.1, 2017, p. 29.
13. BOANINI, E., GAZZANO, M., BIGI, A., Acta Biomater., **6**, 2010, p. 1882.
14. TAO, Z.S., ZHOU, W.S., HE, X.W., LIU, W., BAI, B.L., ZHOU, Q., HUANG, Z.L., TU, K.K., LI, H., SUN, T., LV, Y.X., CUI, W., YANG, L., Mater. Sci. Eng. C, **62**, 2016, p. 226.
15. HUANG, Y., QIAO, H., NIAN, X., ZHANG, X., ZHANG, X., SONG, G., XU, Z., ZHANG, H., HAN, S., Surf. Coat. Technol., **291**, 2016, p. 205.
16. HUANG, Y., HAO, M., NIAN, X., QIAO, H., ZHANG, X., ZHANG, X., SONG, G., GUO, J., PANG, X., ZHANG, H., Ceram. Int., **42**, 2016, p. 11876.
17. TOMOAIA, G., TOMOAIA-COTISEL, M., POP, L.B., POP, A., HOROVITZ, O., MOCANU, A., JUMATE, N., BOBOS, L.D., Rev. Roum. Chim., **56**, nr. 10-11, 2011, p. 1039.
18. TOMOAIA, G., SORITAU, O., TOMOAIA-COTISEL, M., POP, L.B., POP, A., MOCANU, A., HOROVITZ, O., BOBOS, L.D., Powder Technol., **238**, 2013, p. 99.
19. TOMOAIA, G., TOMOAIA-COTISEL, M., POP, L.B., MOCANU, A., POP, A., Romania, Patent nr.125817, BOPI, nr. 6, 2013, p. 123.
20. MOCANU, A., FURTOS, G., RAPUNTEAN, S., HOROVITZ, O., FLORE, C., GARBO, C., DANISTEANU, A., RAPUNTEAN, G., PREJMEREAN, C., TOMOAIA COTISEL
21. GOGA, F., FORIZS, E., AVRAM, A., ROTARU, A., LUCIAN, A., PETEAN, I., MOCANU, A., TOMOAIA-COTISEL, M., Rev. Chim. (Bucuresti), **68**, no. 6, 2017, p. 1193
22. AINA, V., LUSVARDI, G., ANNAZ, B., GIBSON, I.R., IMRIE, F.E., MALAVASI, G., MENABUE, L., CERRATO, G., MARTRA, G., J. Mater. Sci: Mater. Med., **23**, 2012, p. 2867.
23. KAYGILI, O., KESER, S., Mater. Lett., **141**, 2015, p. 161.
24. MOREIRA, M.P., DE ALMEIDA SOARES, G.D., DENTZER, J., ANSELME, K., DE SENA, L.A., KUZNETSOV, A., DOS SANTOS, E.A., Mater. Sci. Eng. C, **61**, 2016, p. 736.
25. HOROVITZ, O., TOMOAIA, G., MOCANU, A., YUPSANIS, T., TOMOAIA-COTISEL, M., Gold Bull., **40**, nr.4, 2007, p. 295.
26. TOMOAIA, G., FRANGOPOL, P.T., HOROVITZ, O., BOBOS, L.D., MOCANU, A., TOMOAIA-COTISEL, M., J. Nanosci. Nanotechnol., **11**, nr. 9, 2011, p. 7762.
27. TOMOAIA-COTISEL, M., TOMOAIA-COTISEL, A., YUPSANIS, T., TOMOAIA, G., BALEA, I., MOCANU, A., RACZ, C., Rev. Roum. Chim., **51**, nr. 12, 2006, p. 1181.
28. TOMOAIA, G., POP, L.B., PETEAN, I., TOMOAIA-COTISEL, M., Mat. Plast., **49**, no. 1, 2012, p. 48.
29. GOPI, D., SHINYJOY, E., KAVITHA, L., Ceram. Int., **41**, 2015, p. 5454.
30. PANG, Y.X., BAO, X., J. Eur. Ceram. Soc., **23**, 2003, p. 1697.
31. HABERKO, K., BUCKO, M.M., BRZEZINSKA-MIECZNIK, J., HABERKO, M., MOZGAWA, W., PANZ, T., PYDA, A., ZAREBSKI, J., J. Eur. Ceram. Soc., **26**, 2006, p. 537.
32. TANAKA, H., CHIKAZAWA, M., KANDORI, K., ISHIKAWA, T., Phys. Chem. Chem. Phys., **2**, 2000, p. 2647.
33. KANNAN, S., LEMOS, I.A.F., ROCHA, J.H.G., FERREIRA, J.M.F., J. Solid State Chem., **178**, 2005, p. 3190.
34. ASHOK, M., SUNDARAM, N.M., KALKURA, S.N., Mater. Lett., **57**, nr. 13-14, 2003, p. 2066.
35. KIM, H.W., KOH, Y.H., KONG, Y.M., KANG, J.G., KIM, H.E., J. Mater. Sci. Mater. Med., **15**, 2004, p. 1129.
36. RENAUDIN, G., JALLOT, E., NEDELEC, J.M., J. Sol-Gel Sci. Technol., **51**, 2009, p. 287.
37. LIAO, C.J., LIN, F.H., CHEN, K.S., SUN, J.S., Biomaterials, **20**, 1999, p. 1807.
38. MA, M., ZHANG, B., LU, W., LIU, J., GUO, Y., Chin. Sci. Bull., **59**, nr. 7, 2014, p. 606.
39. BATRA, U., KAPOOR, S., SHARMA, S., J. Mater. Eng. Perform., **22**, nr.6, 2013, p. 1798.

Manuscript received: 14.05.2017